Self-Assembly and Selective Guest Binding of Three-Dimensional Open-Framework Solids from a Macrocyclic Complex as a Trifunctional Metal Building Block

Kil Sik Min and Myunghyun Paik Suh*[a]

Abstract: The nickel(II) hexaazamacrocyclic complex (**1**) containing pendant pyridine groups has been synthesized by the one-pot template condensation reaction of amine and formaldehyde. From the self-assembly of **1** with deprotonated *cis,cis*-1,3,5-cyclohexanetricarboxylic acid, H_2CTC^- and CTC^{3-}, three-dimensional supramolecular open-frameworks of $[Ni(C_{20}H_{32}N_8)][C_6H_9(COOH)_2(COO)]_2 \cdot 4H_2O$ (**2**) and $[Ni(C_{20}H_{32}N_8)]_3[C_6H_9(COO)_3]_2 \cdot 16H_2O$ (**3**), respectively, have been constructed. The solids **2** and **3** are insoluble in all solvents. X-ray crystal structure of **2** indicates that each nickel(II) macrocyclic complex binds two H_2CTC^- ions in *trans* position and two pendant pyridine groups of the macrocyclic complex are involved in hydrogen-bonding interactions with the hydroxy groups of H_2CTC^- belonging to the neighboring macrocyclic complexes, which provides the beltlike one-dimensional chain composed of rectangular synthons. The one-dimensional chains are linked together through lattice water molecules by the hydrogen-bonding interactions to generate two-dimensional networks, which are again connected to each other by the offset $\pi-\pi$ stacking interactions between the pendant pyridine rings to give rise to a three-dimensional structure in which channels are present. The X-ray crystal structure of **3** indicates that each nickel(II) macrocyclic unit binds two CTC^{3-} ions in *trans* position and each CTC^{3-} ion coordinates three nickel(II) macrocyclic complexes to form a two-dimensional layer, in which pendant pyridine rings are involved in the hydrogen bonding and the herringbone $\pi-\pi$ interaction. Between the layers, the pendant pyridine rings belonging to the neighboring layers participate in the offset $\pi-\pi$ stacking interactions, which gives rise to a three-dimensional network structure. The network creates channels running parallel to the *a*, *b*, and *c* axes, which are filled with guest water molecules. The X-ray powder diffraction patterns indicate that the frameworks of **2** and **3** are deformed upon removal of water guests but restored upon rebinding of water. The host solids **2** and **3** bind $[Cu(NH_3)_4](ClO_4)_2$ in MeCN with a binding constant (K_f) of $210\,M^{-1}$ and $710\,M^{-1}$, respectively, while they do not bind $[Cu(en)_2](ClO_4)_2$ (en = ethylenediamine). The dried solids of **2** and **3** do not interact with benzene and toluene, but they differentiate methanol, ethanol, and phenol in toluene solvent with the K_f values of 42, 14, and $12\,M^{-1}$, respectively, for **2**, and 13, 8.2, and $8.9\,M^{-1}$, respectively, for **3**. In terms of binding sites for guest molecules, the solid **3** has greater capacity than the solid **2**.

Keywords: host–guest chemistry · hydrogen bonds · macrocyclic ligands · stacking interactions · supramolecular chemistry

Introduction

Much effort has been invested in the attempts at the design and synthesis of metal-organic coordination networks having specific network topologies and potentially interesting properties.[1–12] Self-assembly of organic molecules and metal-ion building blocks may yield multidimensional networks containing channels or cavities of various sizes and shapes, which can be applied in adsorption and separation processes as well as in catalysis.[13–18] However, the supramolecules with large cavities are often interpenetrated or catenated and become condensed materials in the solid state.[19] Furthermore, the frameworks of the solids containing pores or channels often collapse upon removal of guest inclusions due to the crystal packing forces. To become a useful new class of molecular-based material, the solid should sustain its cavities even after the removal of the guests, or be able to restore them upon guest binding. Therefore, the rational design and construction of open frameworks with proper building blocks is very important.

[a] Prof. Dr. M. P. Suh, K. S. Min
School of Chemistry & Molecular Engineering
and Center for Molecular Catalysis
Seoul National University, Seoul 151-747 (Republic of Korea)
Fax: (+82) 2-886-8516
E-mail: mpsuh@snu.ac.kr

Supporting information for this contribution is available on the WWW under http://www.wiley-vch.de/home/chemistry.

  0947-6539/01/0701-0303 $ 17.50+.50/0

In the self-assembly of supramolecular networks, macrocyclic complexes have seldom been employed as metal building blocks.[20,21] Previously, we constructed three-dimensional networks of the molecular brick-wall and honeycomb-type from a macrocyclic complex containing pendant hydroxy groups and 1,3,5-benzenetricarboxylate.[20] In these networks, the macrocyclic complex acts as a bifunctional building block, involving metal–ligand coordination and the hydrogen-bonding interactions. However, they were not robust. They lost crystallinity upon exposure to the air and dissociated into the building blocks upon dissolution in water.

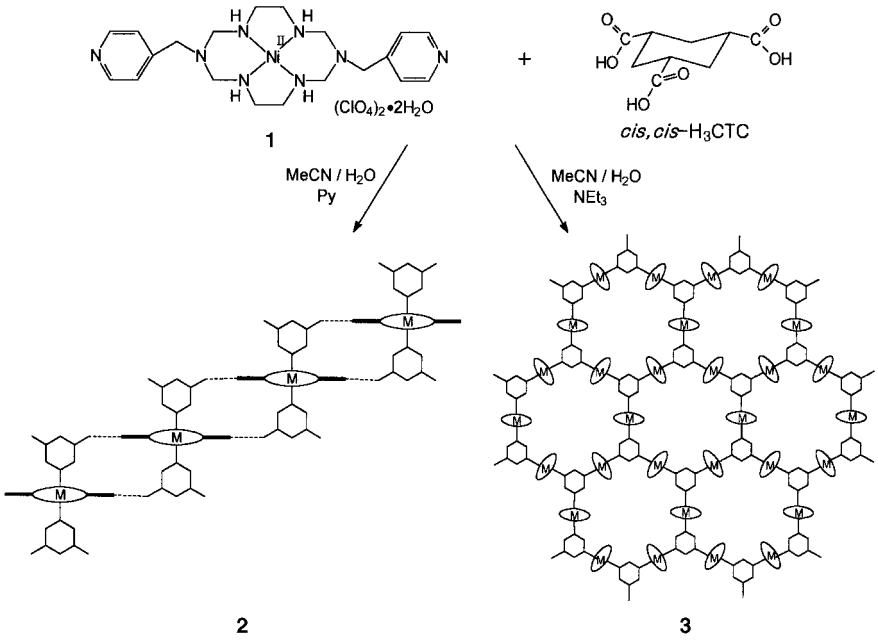

Scheme 1. Self-assembly of **1** with H_2CTC^- and CTC^{3-}.

To build more robust and insoluble three-dimensional open frameworks, we have synthesized the nickel(II) macrocyclic complex containing pyridyl pendant chains, $[Ni(L^1)](ClO_4)_2 \cdot 2H_2O$ (**1**) (Scheme 1), as a *trifunctional* metal building block. We expected that the complex would induce extensive hydrogen bonding and $\pi-\pi$ stacking interactions as well as metal–ligand coordination, so that the solid constructed from it may become robust. In the self-assembly of **1** with *cis,cis*-1,3,5-cyclohexanetricarboxylic acid (H_3CTC) in the presence of base, we have constructed two different three-dimensional networks. Depending upon the degree of deprotonation of H_3CTC, we have obtained three-dimensional networks $[Ni(C_{20}H_{32}N_8)][C_6H_9(COOH)_2(COO)]_2 \cdot 4H_2O$ (**2**), which consists of linear chains with rectangular synthons, and $[Ni(C_{20}H_{32}N_8)]_3[C_6H_9(COO)_3]_2 \cdot 16H_2O$ (**3**), which consists of puckered honeycomb-like sheets (Scheme 1). The solids **2** and **3** are insoluble solids and contain cavities and channels, which are deformed upon removal of water guests but restored upon rebinding of the guests. They selectively bind $[Cu(NH_3)_4](ClO_4)_2$ in MeCN over $[Cu(en)_2](ClO_4)_2$. They bind the organic guests such as MeOH, EtOH, and PhOH with different binding constants. Herein we report syntheses, structures, and properties of **1**–**3** and the selective guest binding of **2** and **3**.

Abstract in Korean:

피리딘기를 갖는 니켈(II) 헥사아자 거대고리 착물을(**1**) 아민과 포름알데히드의 주형축합반응에 의해서 합성하였다. 착물 **1** 은 탈양성자화된 시스,시스-1,3,5-시클로헥산카르복실산, 즉 H_2CTC^- 및 CTC^{3-}과 자기조립하여 3차원 그물구조 초분자 $[Ni(C_{20}H_{32}N_8)][C_6H_9(COOH)_2(COO)]_2 \cdot 4H_2O$ (**2**) 와 $[Ni(C_{20}H_{32}N_8)]_3[C_6H_9(COO)_3]_2 \cdot 16H_2O$ (**3**)을 형성한다. 고체 **2** 와 **3** 은 어떤 용매에도 녹지 않는다. **2** 의 X-선 결정구조에 의하면 각각의 니켈(II) 거대고리 착물에 두개의 H_2CTC^- 이온이 트란스 위치로 배위되고, 거대고리 착물의 피리딘기들은 이웃하는 거대고리 착물에 배위된 H_2CTC^- 이온의 히드록시기와 수소결합을 하여 일차원 사슬을 이룬다. 일차원 사슬들은 격자 물분자와의 수소결합으로 연결되어 이차원 그물구조를 가지며, 다시 피리딘기들 간의 어긋남 $\pi-\pi$ 쌓임 상호작용에 의해 결국 삼차원 구조를 갖게 된다. **3** 의 X-선 결정구조에 의하면 각각의 니켈(II) 거대고리 착물에는 두개의 CTC^{3-} 이온이 트란스 위치로 배위되고 CTC^{3-} 이온은 세개의 니켈(II) 거대고리 착물을 배위함으로써 이차원 층을 이룬다. 피리딘기는 이차원 층 내에서 수소결합 및 $\pi-\pi$ 빗살무늬 쌓임 상호작용을 하고 층간에는 어긋남 $\pi-\pi$ 쌓임 상호작용을 함으로써 삼차원 그물구조를 형성한다. 이 구조는 *a*, *b*, 그리고 *c* 축을 따라서 통로를 만들고 이 속에 손님 물분자를 가둔다. X-선 분말회절 유형에 의하면 **2** 와 **3** 은 손님분자를 제거하면 구조가 변형되나 물분자를 다시 결합시키면 원래의 구조로 복원된다. 고체 **2** 와 **3** 은 아세토니트릴 용매에서 $[Cu(NH_3)_4](ClO_4)_2$와 결합하며 결합상수(K_f)는 각각 210 M^{-1}와 710 M^{-1}였다. 반면에 $[Cu(en)_2](ClO_4)_2$와는 결합하지 않았다. 건조된 고체 **2** 와 **3** 은 벤젠 및 톨루엔은 결합하지 않는다. 그러나 메탄올, 에탄올, 그리고 페놀은 구별한다. 고체 **2** 에 대한 결합상수는 각각 42, 14, 그리고 12 M^{-1}였다. 고체 **3** 에 대한 결합상수는 각각 13, 8.2, 그리고 8.9 M^{-1}이다. 결합자리를 고려할 때 고체 **3** 이 고체 **2** 보다 손님분자 수용량은 더 크다.

Results and Discussion

Synthesis and X-ray structure of $[Ni(L^1)](ClO_4)_2 \cdot 2H_2O$ (1): The macrocyclic complex **1** was prepared as a building block for the construction of three-dimensional networks. The complex was synthesized in MeOH by the one-pot template condensation reaction of ethylenediamine, formaldehyde, and 4-(aminomethyl)pyridine in the presence of nickel(II) ion. The synthetic method was modified from those previously developed in our laboratory.[22–25] The complex was isolated from the reaction mixture by protonating the pyridyl nitrogen atoms of the macrocycle with the acid. The protonated compound was treated with triethylamine to obtain **1**. The compound **1** is soluble in DMF, Me_2SO, MeCN, $MeNO_2$, and hot H_2O.

An ORTEP drawing for the cation of **1** is shown in Figure 1 a. Table 1 gives selected bond lengths and angles. The nickel(II) ion displays a square-planar coordination geometry by binding to the four secondary nitrogen donors of the

0947-6539/01/0701-0304 $ 17.50+.50/0 *Chem. Eur. J.* **2001**, *7*, No. 1

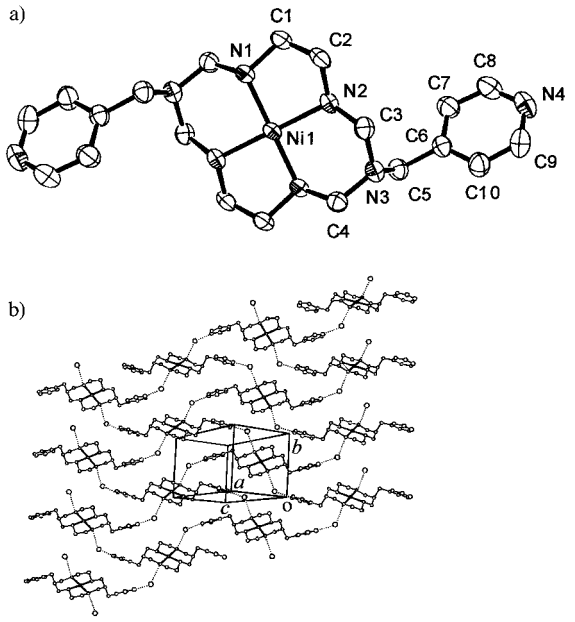

Figure 1. a) An ORTEP view of the cation of **1** with atomic numbering scheme (thermal ellipsoids at 40% probability). b) The two-dimensional network of **1** formed by hydrogen bonding. Hydrogen bonds are indicated as by $\cdots$ lines.

Table 1. Selected bond lengths [Å] and angles [°] for **1**.[a]

Ni1–N1	1.934(3)	N4–C9	1.323(7)
Ni1–N2	1.934(3)	C1–C2	1.487(6)
N1–C1	1.487(5)	C4–N1′	1.501(5)
N2–C2	1.480(5)	C5–C6	1.496(5)
N2–C3	1.493(5)	C6–C10	1.369(6)
N3–C3	1.435(5)	C6–C7	1.377(6)
N3–C4	1.434(5)	C7–C8	1.384(7)
N3–C5	1.473(5)	C9–C10	1.367(7)
N4–C8	1.311(7)		
N1-Ni1-N2	86.52(13)	C2-C1-N1	106.3(3)
N1-Ni1-N2′	93.48(13)	N2-C2-C1	106.7(3)
C1-N1-C4′	110.8(3)	N3-C3-N2	114.8(3)
C1-N1-Ni1	108.4(2)	N3-C4-N1′	113.7(3)
Ni1-N1-C4′	117.2(3)	N3-C5-C6	111.7(3)
C2-N2-C3	111.3(3)	C10-C6-C7	116.6(4)
C2-N2-Ni1	108.3(2)	C10-C6-C5	121.7(4)
C3-N2-Ni1	117.7(2)	C7-C6-C5	121.7(4)
C3-N3-C4	113.4(3)	C6-C7-C8	118.8(5)
C3-N3-C5	115.1(3)	N4-C8-C7	124.0(5)
C4-N3-C5	114.4(3)	N4-C9-C10	122.6(5)
C8-N4-C9	117.1(4)	C6-C10-C9	120.9(5)

[a] Symmetry transformations used to generate equivalent atoms: ′: $-x$, $-y$, $-z$.

macrocycle at an average Ni–N bond length of 1.934(3) Å. The pendant pyridine groups of the macrocycle are not involved in either intra- or intermolecular coordination of metal ion. The complex possesses an inversion center at the nickel atom. The macrocyclic ligand adopts thermodynamically the most stable *R*,*R*,*S*,*S* (*trans*-III) configuration,[26] and thus the pyridyl pendants are positioned above and below the square coordination plane. The six-membered chelate rings adopt a chair conformation and the five-membered chelate rings assume a *gauche* conformation. The C–N bond lengths and the C-N-C angle involving the bridgehead tertiary nitrogen atom N3 are 1.447(3) Å (av) and 113–115°, respectively, indicating significant contribution of sp^2 hybridization of the bridgehead nitrogen atoms.[22–25] The pendant pyridine groups of the macrocycle are involved in the hydrogen-bonding interaction with lattice water molecules: N4$\cdots$$O_{W1}$ 2.818(6) Å, N4-H_{W2}-O_{W1} 178.4°. In addition, the oxygen atoms of the lattice water molecules interacting with the pyridyl pendants of a macrocycle act as hydrogen acceptors to form additional hydrogen bonds with secondary amines of the neighboring macrocycle: $O_{W1}\cdots$N1 2.908(5) Å, O_{W1}-H1-N1 135.2°. Owing to these hydrogen-bonding interactions, all the macrocyclic complexes are linked together, resulting in a two-dimensional network (Figure 1b). Perchlorate anions are located between the two-dimensional sheets and the oxygen atom of the perchlorate ion forms a hydrogen bond with the secondary amine of the macrocycle (O1($x-1$, y, z)$\cdots$N2 3.080(6) Å, O1-H2-N2 157.1°).

Self-assembly and properties of three-dimensional open frameworks 2 and 3: The self-assembly of **2** and **3** is schematically described in Scheme 1. Our synthetic strategy for the three-dimensional open frameworks was based on the metal–ligand coordination between **1** and the carboxylate anion derived from *cis*,*cis*-1,3,5-cyclohexanetricarboxylic acid (H_3CTC) as well as on hydrogen bonding and $\pi-\pi$ stacking interactions[27] induced by the pendant pyridyl groups of **1**. In the self-assembly in MeCN/H_2O (1/1 v/v), pyridine or triethylamine was added as a base to deprotonate H_3CTC. When pyridine was used as a base, H_2CTC^- underwent a self-assembly reaction with **1** to generate the three-dimensional network of **2**. When triethylamine was used as a base, CTC^{3-} underwent a self-assembly reaction with **1** to generate the three-dimensional network of **3**. The supramolecular solids **2** and **3** are pink and they never lose guest water molecules in the air at room temperature and maintain their crystallinity. Furthermore, they are completely insoluble in water and in organic solvents such as MeCN, MeOH, EtOH, $MeNO_2$, $CHCl_3$, THF, DMF, DMSO, toluene, acetone, hexane, and benzyl alcohol. However, when solids **2** and **3** (20 mg) were immersed in an aqueous solution of 0.1M $HClO_4$ (1 mL) they dissolved immediately into the solution and dissociated into the building blocks, giving rise to a yellow solution. When **2** and **3** (20 mg) were added to an aqueous solution of 0.1M NaOH (1 mL), they dissolved slowly into the solution to provide a pink solution.

The diffuse reflectance spectra of **2** and **3** show maximum absorptions at 267, 335, 507, and 640 nm and at 260, 332, 509, and 655 nm, respectively; these are the characteristic chromophores for the nickel(II) ion coordinated with N_4O_2 donors.[28]

Molecular-based materials that can sustain their frameworks even after the removal of guest molecules are very important in view of the development of new classes of porous substances. The thermogravimetric analysis (TGA) trace of **2** (Figure 2a) shows a weight loss of 7.6% at 94°C, which corresponds to the loss of four guest water molecules per unit formula. No chemical decomposition was observed up to 200°C. The TGA trace of **3** (Figure 2b) shows a weight loss of 14.6% at 85°C, corresponding to the loss of sixteen guest water molecules per unit formula. No chemical decomposi-

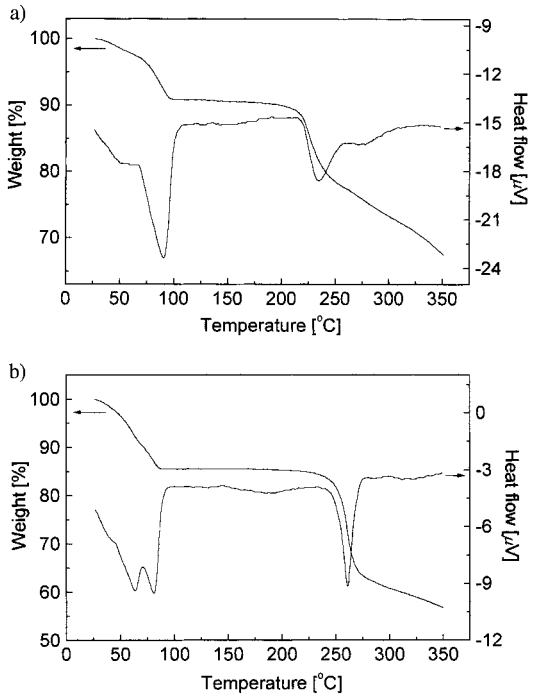

Figure 2. a) Thermogravimetric analysis (TGA) and differential thermal analysis (DTA) traces for **2**. b) TGA and DTA traces for **3**.

tion was observed up to 225 °C. The X-ray powder diffraction (XRPD) patterns (see Figure 3d and Figure 4d) for the solids **2** and **3**, which were heated at 140 and 170 °C, respectively, revealed that they had turned into other crystalline forms.

The XRPD patterns of **2** and **3** as prepared and the desolvated solids are compared in Figure 3 and Figure 4, respectively. Although the desolvated solids maintain the

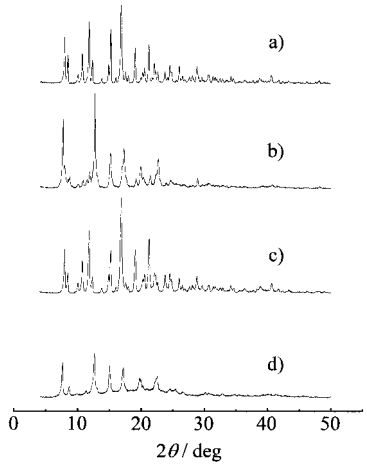

Figure 3. The XRPD patterns of: a) original solid **2**, $[Ni(C_{20}H_{32}N_8)][C_6H_9(COOH)_2(COO)]_2 \cdot 4H_2O$; b) dried solid (at 90 °C for 3 h), $[Ni(C_{20}H_{32}N_8)][C_6H_9(COOH)_2(COO)]_2$; c) solid obtained by immersing b in 1:1 H_2O/MeCN for 10 min; d) solid **2** heated at 140 °C for 30 min.

crystal morphologies as observed under a microscope, their XRPD patterns show different peak positions and intensities compared with those of the original crystals. However, when the dried solids were immersed in a mixture of MeCN/H_2O (1/1 v/v) for 10 min, XRPD patterns fully coincident with

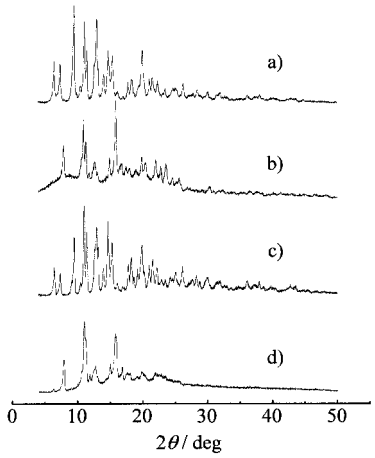

Figure 4. The XRPD patterns of: a) original solid **3**, $[Ni(C_{20}H_{32}N_8)]_3[C_6H_9(COO)_3]_2 \cdot 16H_2O$; b) dried solid (at 80 °C for 3 h under vacuum), $[Ni(C_{20}H_{32}N_8)]_3[C_6H_9(COO)_3]_2$. c) solid obtained by immersing b in 1:1 H_2O/MeCN for 10 min. d) solid **3** heated at 170 °C for 30 min.

those observed for the original solids were regenerated. In addition, when water vapor was diffused into the dehydrated solids of **2** and **3**, respectively, the XRPD patterns (see Figures S1 and S2 in the Supporting Information) were also regenerated for **2** and **3**. The three-dimensional networks **2** and **3** constructed by the highly cooperative hydrogen bonding and $\pi-\pi$ stacking interactions, as verified by the X-ray crystal structures, are sufficiently robust for the reversible exclusion and inclusion of the guest water molecules. The dried solids of **2** and **3** may be applied as adsorbents of water and water vapor.

X-ray crystal structure of $[Ni(C_{20}H_{32}N_8)][C_6H_9(COOH)_2(COO)]_2 \cdot 4H_2O$ (2): An ORTEP drawing of the fundamental building unit of **2** is shown in Figure 5a. Table 2 shows the selected bond lengths and angles. The coordination geometry around the nickel(II) ion is a tetragonally distorted octahedron in which the nickel(II) ion is coordinated to the four secondary

Table 2. Selected bond lengths [Å] and angles [°] for **2**.[a]

Ni1−N1	2.068(2)	C7−C8	1.378(4)
Ni1−N3	2.049(2)	C9−C10	1.391(5)
Ni1−O1	2.147(2)	O1−C11	1.258(3)
N1−C1	1.471(3)	O2−C11	1.255(3)
N1−C2	1.484(3)	O3−C12	1.199(5)
N4−C8″	1.320(5)	O4−C12	1.306(4)
N4−C9″	1.320(5)	C4−C1′	1.515(4)
C1−C4′	1.515(4)	C5−C6	1.513(4)
C6−C7	1.380(4)	O5−C13	1.211(4)
C6−C10	1.383(4)	O6−C13	1.310(4)
N1-Ni1-N3	94.08(8)	O5-C13-O6	122.7(3)
N1′-Ni1-N3	85.92(8)	N4‴-C8-C7	123.0(3)
N1-Ni1-O1	93.41(7)	N4‴-C9-C10	123.6(3)
N3-Ni1-O1	87.24(7)	C6-C10-C9	118.4(3)
C1-N1-Ni1	104.71(14)	C11-O1-Ni1	134.1(2)
C2-N1-Ni1	113.23(15)	O1-C11-O2	124.6(2)
C3-N3-Ni1	113.74(14)	O1-C11-C14	118.8(2)
C4-N3-Ni1	105.77(14)	O2-C11-C14	116.6(2)
C8″-N4-C9″	117.7(3)	O3-C12-O4	123.1(3)
O4-C12-C16	112.8(3)	O3-C12-C16	123.8(3)
O5-C13-C18	123.5(3)	O6-C13-C18	113.7(2)

[a] Symmetry transformations used to generate equivalent atoms: ′: $-x+1, -y, -z$; ″: $x, y+1, z$; ‴: $x, y-1, z$.

0947-6539/01/0701-0306 $ 17.50+.50/0 *Chem. Eur. J.* **2001**, *7*, No. 1

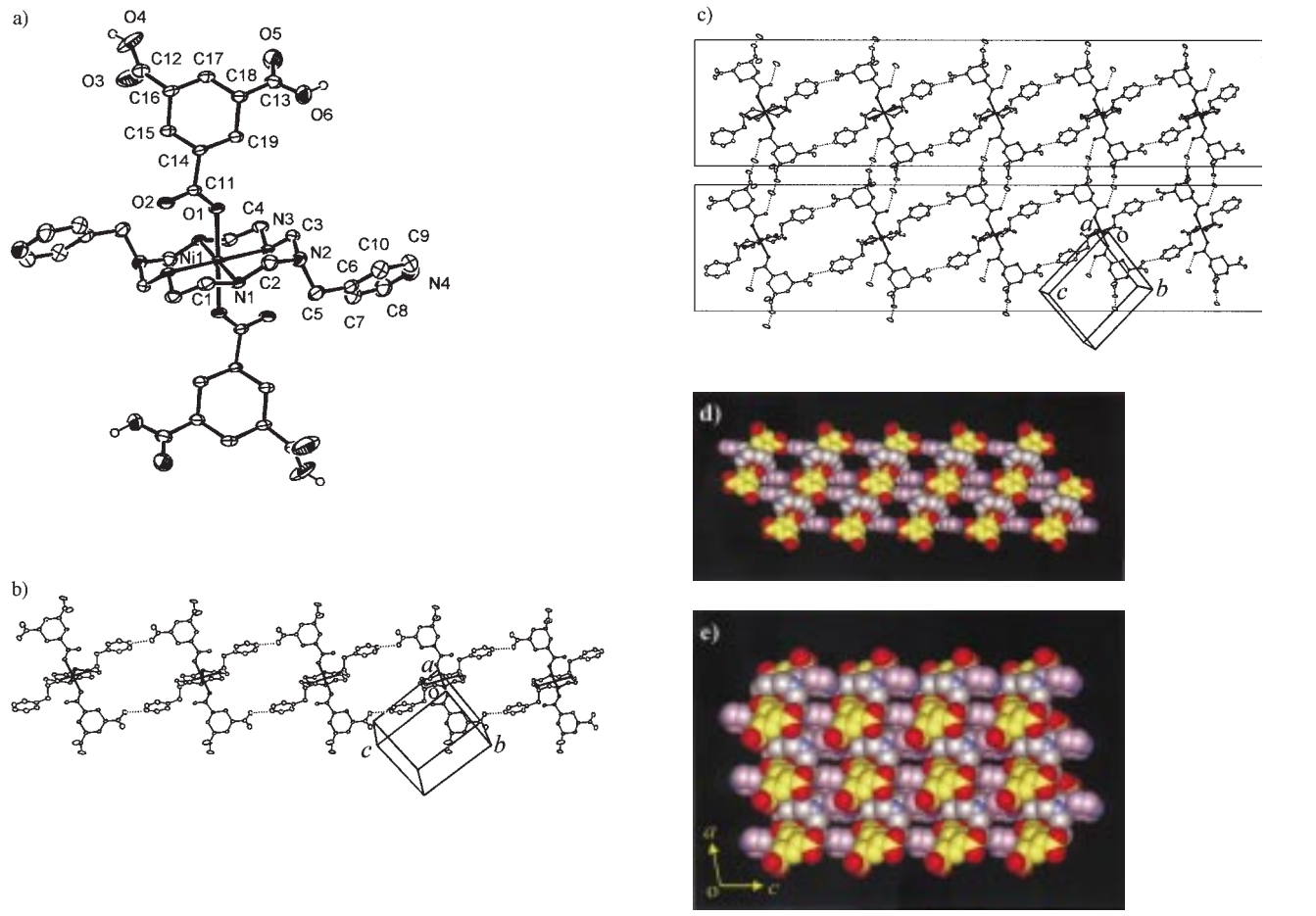

Figure 5. a) An ORTEP view of the cation of **2** with atomic numbering scheme (thermal ellipsoids at 50% probability). b) A one-dimensional chain of **2**. c) A two-dimensional sheet formed by hydrogen-bonding interactions between one-dimensional chains. Hydrogen bonds are indicated by ··· lines. d) A CPK representation showing offset $\pi-\pi$ stacking interactions between the two one-dimensional chains of **2**. The effective void size is about 3.8×9.8 Å. e) CPK representation of the three-dimensional network of **2**. (white: nickel(II) ion, red: oxygen, blue: nitrogen, violet: carbon of pyridine, gray: carbon of macrocycle, yellow: carbon of H_2CTC^-).

nitrogen atoms of the macrocycle as well as to two oxygen atoms of two H_2CTC^- ions located *trans*. The average Ni–N and Ni–O bond lengths are 2.059(1) and 2.147(2) Å, respectively. The nickel(II) macrocyclic complexes are linked together to form a three-dimensional network. The two pendant pyridine groups of each macrocyclic complex are involved in hydrogen-bonding interactions with the hydroxy groups of H_2CTC^- coordinating the neighboring macrocyclic complexes: N4···O6 $(-x+1, -y, -z+1)$ 2.658(3) Å, N4-H6-O6 174.4°. This creates rectangular supramolecular synthons (Figure 5b), which are linked together to form a one-dimensional chain extending along $[01\bar{1}]+1/2a$ direction by sharing the opposite corners of the rectangles. The Ni···Ni distance in the rectangular synthon is 14.435(2) Å and the effective size of the rectangular cavity is 3.8×9.8 Å as measured by the van der Waals surface of the opposing wall. The cavities are filled with water guest molecules. Within a one-dimensional chain, the free carbonyl oxygen atom of the coordinated carboxylate forms intramolecular hydrogen bonds with a secondary amine of the macrocycle (O2···N3$(-x+1, -y, -z)$ 2.893(3) Å, O2-H3-N3 148.5°) as well as with a lattice water molecule (O2···$O_{W1}(-x+1, -y, -z)$ 2.740(3) Å). The one-dimensional chains are linked together by the hydrogen-bonding and $\pi-\pi$ stacking interactions. In particular, a free carboxylic acid group of H_2CTC^- belonging to a chain forms a hydrogen bond with a lattice water molecule (O_{W1}): (O4···O_{W1} $(x+1, y-1, z-1)$ 2.632(4) Å, O4-H4-O_{W1} 162.9°) which again interacts with the free carbonyl oxygen atom of the coordinated carboxylate group belonging to the neighboring chain (O4···$O_{W1}(x+1, y-1, z-1)$ 2.632(4) Å, O_{W1}···O2$(-x+2, -y-1, -z-1)$ 2.740(3) Å, O4-O_{W1}-O2, 113.4°), which leads to the two-dimensional network extending along the (211) plane (Figure 5c). The two-dimensional layers are connected together by the offset $\pi-\pi$ stacking interactions[27] between the pendant pyridine rings (Figure 5d). The pyridine rings are positioned parallel ($\theta = 0.0°$) to each other, with an interplanar separation of 3.50–3.52 Å. The offset angle between the pyridine ring planes is 28.6°. The offset $\pi-\pi$ stacking interactions between the two-dimensional sheets extend along the (222) plane. Owing to these interchain interactions, compound **2** becomes a three-dimensional network, which generates channels as shown in Figure 5e. The void volume of the cavities in a unit cell is 106 Å^3, which equals 9.7% of the unit cell volume.[29]

X-ray crystal structure of $[Ni(C_{20}H_{32}N_8)]_3[C_6H_9(COO)_3]_2 \cdot 16H_2O$ (3): An ORTEP view of the fundamental building unit of **3** is shown in Figure 6a. Table 3 gives the selected bond lengths and angles. The coordination geometry around the nickel(II) ion is a tetragonally distorted octahedron. The nickel(II) ion is coordinated to four secondary amine donors of the macrocycle as well as to two oxygen atoms from two CTC^{3-} ions. The average Ni–N and Ni–O bond lengths are 2.049(2) and 2.147(2) Å, respectively. Since each nickel(II) ion is coordinated to two CTC^{3-} ions and each CTC^{3-} binds to three nickel(II) macrocyclic units, the stoichiometry of the network is $Ni^{2+}/CTC^{3-} = 3:2$, which generates two-dimensional layers extending along the $(11\bar{1})$ plane. The metal–metal distances around CTC^{3-} are NiA···NiB 8.127(2), NiA···NiC 9.813(2), and NiB···NiC 8.703(2) Å. Since the cyclohexane ring of CTC^{3-} has a chair conformation, the two-dimensional layer is not flat. In the structure of the two-dimensional sheet, six nickel(II) macrocyclic complexes and six CTC^{3-} form a ring, which is a basic motif of the molecule (Figure 6b). The effective size of the cavities in a two-dimensional layer is estimated as 4.0 Å × 8.5 Å. Three of the six macrocyclic complexes and three of the six CTC^{3-} ligands are located above and the rest are positioned below the mean plane. The two-dimensional network is reinforced with the hydrogen-bonding and π–π stacking interactions. The uncoordinated carbonyl oxygen atoms of CTC^{3-} form intramolecular hydrogen bonds with secondary amines of the macrocycle: N2A···O2A $(-x, -y, -z)$ 2.903, N2B···O2B$(-x+1, -y, -z+1)$ 2.847 N1C···O2C$(-x+1, -y-1, -z)$ 2.944 Å, N-H-O 149.9–153.0°. The free C=O bond lengths of CTC^{3-} (1.239–1.267 Å) are therefore comparable to those of coordinated C–O bond lengths (1.218–1.258 Å). The pendant pyridyl groups are involved in extensive π–π

Table 3. Selected bond lengths [Å] and angles [°] for **3**.

NiA–N1A	2.075(5)	NiC–O1C	2.186(3)
NiA–N2A	2.066(4)	C7–O1A	1.245(6)
NiA–O1A	2.096(3)	C7–O2B	1.239(6)
NiB–N1B	2.066(4)	C8–O1B	1.218(6)
NiB–N2B	2.029(4)	C8–O2B	1.267(6)
NiB–O1B	2.160(3)	C9–O1C	1.258(7)
NiC–N1C	2.017(6)	C9–O2C	1.249(7)
NiC–N2C	2.013(6)		
N1A-NiA-N2A	86.11(18)	C9-O1C-NiC	135.4(4)
N1A-NiA-O1A	89.00(17)	O1A-C7-C1	117.2(4)
N2A-NiA-O1A	86.89(16)	O1A-C7-O2A	125.3(4)
N1B-NiB-N2B	86.54(19)	O2A-C7-C1	117.4(4)
N1B-NiB-O1B	87.93(16)	O1B-C8-C3	118.7(4)
N2B-NiB-O1B	87.35(15)	O1B-C8-O2B	123.2(4)
N1C-NiC-N2C	92.4(3)	O2B-C8-C3	118.0(5)
N1C-NiC-O1C	86.8(2)	O1C-C9-C5	119.1(5)
N2C-NiC-O1C	91.4(2)	O1C-C9-O2C	122.7(5)
C7-O1A-NiA	135.3(3)	O2C-C9-C5	118.2(5)
C8-O1B-NiB	133.9(3)		

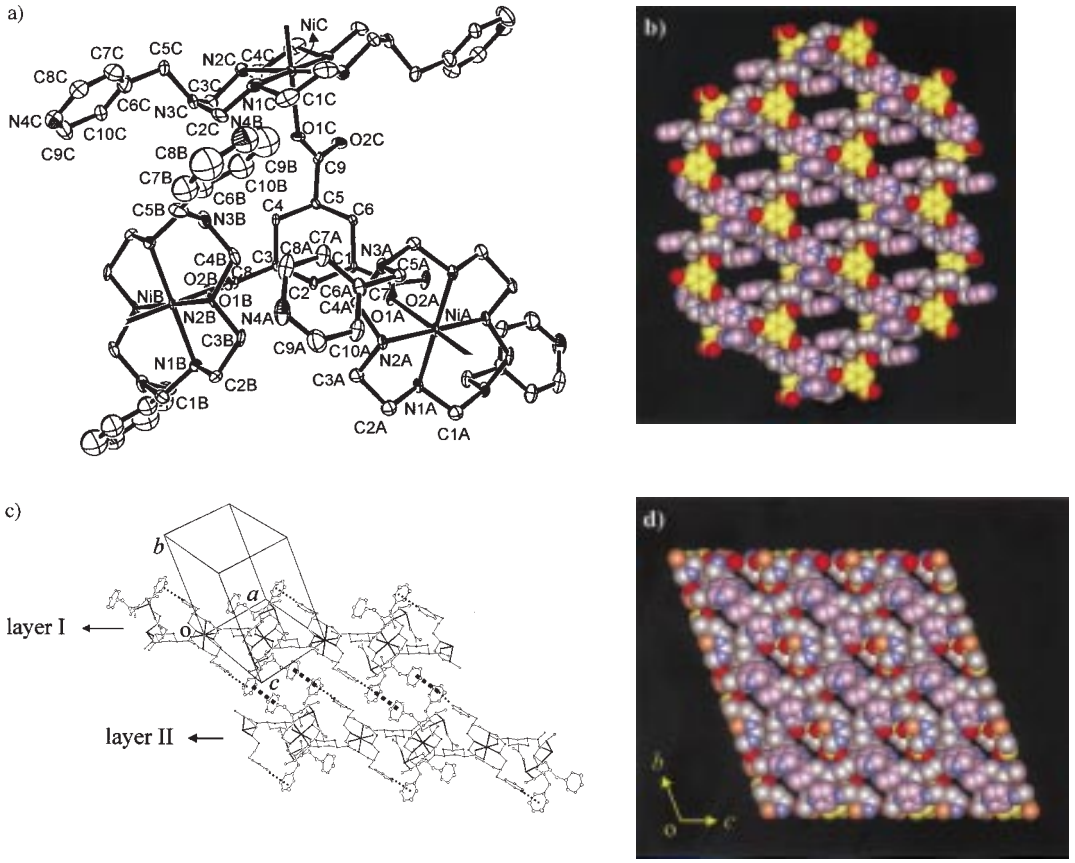

Figure 6. a) An ORTEP view of the trinuclear unit of **3** with atomic numbering scheme (thermal ellipsoids at 15 % probability). b) A CPK representation of a single layer of **3**. The effective size of a void is about 4.0 × 8.5 Å. c) Side view of two-dimensional layers of **3**. The π–π stacking interactions are indicated by ··· lines for intralayer interactions and by ■■■ lines for interlayer interactions. d) CPK view of the packed structure of **3** showing the channels. (orange: nickel(II) ion, red: oxygen, blue: nitrogen, violet: carbon of pyridine, gray: carbon of macrocycle, yellow: carbon of CTC^{3-}).

0947-6539/01/0701-0308 $ 17.50+.50/0 *Chem. Eur. J.* **2001**, *7*, No. 1

stacking interactions. Within a layer, the two pyridine rings involving N4A and N4B are π–π stacked with the herringbone structure: H···centroid 2.699 Å, C-H-centroid 146.9°, centroid···centroid 4.737 Å, dihedral angle between two pyridine rings 83.3°. Between the layers, the pendant pyridine groups involving N4B and N4C located in a layer undergo offset π–π interactions[27] with pyridine groups involving N4C and N4B, respectively, which are positioned in the neighboring layers (Figure 6c). The interplanar separation of the pyridine rings is 3.35–3.64 Å (centroid···centroid, 3.829 Å) and the dihedral angle between the pyridine ring planes is 5.48°. Owing to these interlayer offset π–π interactions, compound **3** becomes a three-dimensional network. The wavelike layers are stacked and separated by 9.241 Å as estimated from the XRPD patterns; the closest metal–metal distance between the layers is 9.537 Å. The packing structure for the multilayers shows that channels are generated in the solid (Figure 6d). The void volume of the cavities in a unit cell is 514 Å^3 (20.8 % of the unit cell volume).[29] The cavities are filled with guest molecules, 16 water molecules per unit formula. Some guest water molecules form hydrogen bonds with free carbonyl oxygen atoms of CTC^{3-} (O2A···$O_{W8}(-x+1, -y, -z)$ 2.730, O2B···O_{W8} 2.677, O2C···$O_{W1}(-x+1, -y, -z)$ 2.802, O2C···$O_{W3}(-x+1, -y, -z)$ 2.744 Å) pyridine pendants of the macrocycle (N4A···O_{W4} $(-x, -y, -z+1)$ 2.969, N4C···O_{W2} $(-x+1, -y, -z+1)$ 3.077 Å), and with the other water inclusions (O_{W1}···O_{W2} 2.732, O_{W1}···O_{W8} 2.834, O_{W4}···O_{W8} $(x-1, y, z)$ 2.870, O_{W6}···$O_{W7}(-x, -y+1, -z)$ 2.676, O_{W6}···O_{W7} 2.714 Å).

Binding of 2 and 3 with copper(II) complexes as guests: When the host solid **2** or **3**, which contains guest water molecules, was immersed in a solution of $[Cu(en)_2](ClO_4)_2$ in MeCN, the absorbance of copper(II) solution did not change, indicating that the solid did not bind the complex. However, in the case of the MeCN solution of $[Cu(NH_3)_4](ClO_4)_2$, the absorbance of the copper(II) solution was reduced and the pale pink color of the host solid changed to blue. The blue color of the solid changed to pale pink when the solid was immersed in water, indicating that binding of the complex was reversible. Since $[Cu(NH_3)_4](ClO_4)_2$ turned into the hydroxide in water, whereas $[Cu(en)_2](ClO_4)_2$ was stable, the binding of the Cu^{II} complexes in the host was measured in MeCN. The perchlorate complexes $[Cu(NH_3)_4](ClO_4)_2$ and $[Cu(en)_2](ClO_4)_2$ were chosen as the guests because they were soluble in MeCN, while $[Cu(en)_2](Cl)_2$ and $[Cu(en)_2](NO_3)_2$ were insoluble in MeCN. The time required to attain equilibrium was estimated by monitoring the changes of the guest concentration spectrophotometrically, and the host solids were immersed in the guest solution until the equilibrium was reached. To obtain K_f and $[BS]_o/\omega$ values for the host–guest complex formation according to Equation (2)(see Experimental Section), the absorbance changes for the MeCN solutions of $[Cu(NH_3)_4](ClO_4)_2$ were measured at 594 nm by varying the initial concentration of the copper(II) complex ($[G]_o$) with the measured amount of the host solid. For complexation of $[Cu(NH_3)_4](ClO_4)_2$ to **2** and **3**, the plots of [BS·G] (the concentration of G bound to BS) against [G] are illustrated in Figure 7. Analysis of the data[30] provides $K_f = 210\,M^{-1}$ for **2**

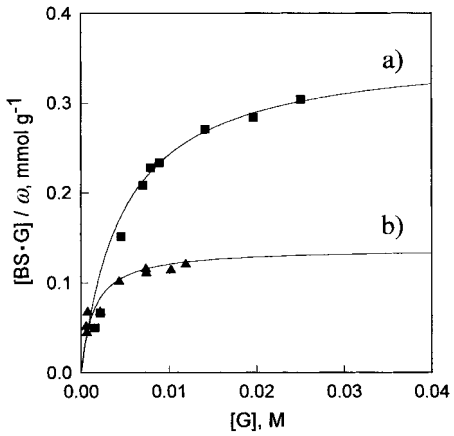

Figure 7. Binding of a) **2** and b) **3** with $[Cu(NH_3)_4](ClO_4)_2$.

and $K_f = 710\,M^{-1}$ for **3** at 25 °C. The values of $[BS]_o/\omega$ indicate that the host solids **2** and **3** have 0.34 and 0.29 binding sites, respectively, for the copper(II) guest molecule per formula weight of the solid. The results are summarized in Table 4. The host–guest compounds were characterized by elemental analysis and IR spectra (see Table S1 and Figures S3–S4 in the Supporting Information) as well as XRPD patterns (Figure 8 and Tables S2 and S3 in the Supporting Information). The host–guest compounds show XRPD patterns in which several peaks appear at the same positions as those of the original crystals, indicating that the host framework structures are maintained even after the inclusion of the copper(II) complex. The selective inclusion of $[Cu(NH_3)_4](ClO_4)_2$ may be attributed to the size-fit of the guest into the channels of the host solid and its better ability to form hydrogen bonds with carbonyl oxygen atoms of H_2CTC^- and CTC^{3-} directed to the inside of the channels. The estimated sizes of $[Cu(NH_3)_4]^{2+}$ and $[Cu(en)_2]^{2+}$ are $5.1 \times 5.1 \times 4.0$ Å^3

Table 4. Inclusion of host solids **2** and **3** with various guests.

Guest	**2**			**3**		
	K_f [M^{-1}]	$[BS]_o/\omega$ [mmol g^{-1}]	guest [mol] included per unit formula of host solid	K_f [M^{-1}]	$[BS]_o/\omega$ [mmol g^{-1}]	guest [mol] included per unit formula of host solid
$[Cu(NH_3)_4](ClO_4)_2$	210 ± 16	0.36 ± 0.01	0.34 ± 0.01[a]	710 ± 55	0.14 ± 0.002	0.29 ± 0.004[a]
MeOH	42 ± 3	6.7 ± 0.1	5.9 ± 0.1[b]	13 ± 0.4	11 ± 0.1	19 ± 0.4[b]
EtOH	14 ± 0.9	4.7 ± 0.1	4.1 ± 0.1[b]	8.2 ± 0.3	7.1 ± 0.1	12 ± 0.2[b]
PhOH	12 ± 0.6	1.3 ± 0.02	1.1 ± 0.02[b]	8.9 ± 0.6	10 ± 0.2	18 ± 0.4[b]

[a] Host solid as prepared. [b] Dried solid.

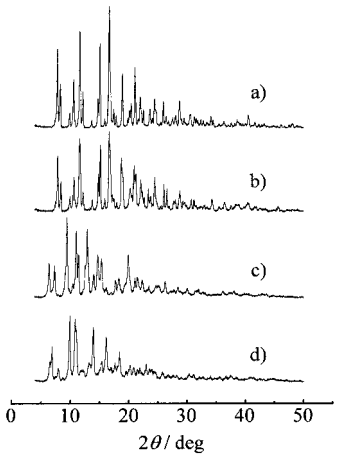

Figure 8. XRPD patterns of a) original solid **2**; b) solid **2** with $[Cu(NH_3)_4](ClO_4)_2$ guest; c) original solid **3**; d) solid **3** with $[Cu(NH_3)_4](ClO_4)_2$ guest.

and $6.5 \times 9.6 \times 4.4$ Å^3, respectively, and the diameter of ClO_4^- is 5.8 Å. The fact that the host solids **2** and **3** selectively bind $[Cu(NH_3)_4](ClO_4)_2$ over $[Cu(en)_2](ClO_4)_2$ also implies that the binding of the copper(II) complex took place in the channels rather than through adsorption on the solid surface.

Inclusion of 2 and 3 with organic guest molecules: When the desolvated host solid **2** or **3** was immersed in toluene containing measured amount of benzene, the concentration of benzene did not change, indicating that benzene molecules were not bound to **2** or **3**. However, when the solid was immersed in a toluene solution containing methanol, ethanol, or phenol, the concentration of the compound changed as measured by GC. The binding of these organic guests in the host solid may be attributed to their hydrogen-bonding interactions as well as to the size-fit with the host cavity. With a measured amount of the host solid, the concentration changes of the organic guest were measured with various initial concentrations of the guest ($[G]_o$), and then the data were fitted to Equation (2) to obtain the K_f value.[30] The plots of $[BS \cdot G]$ (the concentration of G bound to BS) against [G] for the solids **2** and **3** are illustrated in Figures 9 and 10,

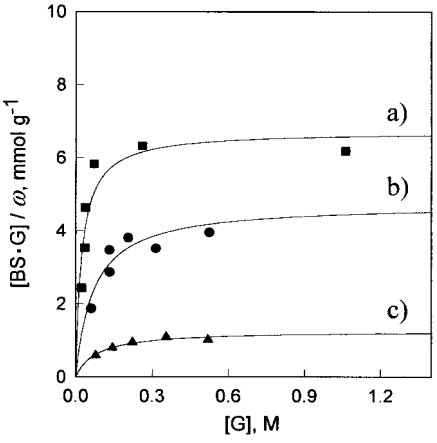

Figure 9. Binding of host solid **2** with organic guests: a) MeOH (■); b) EtOH (●); c) PhOH (▲).

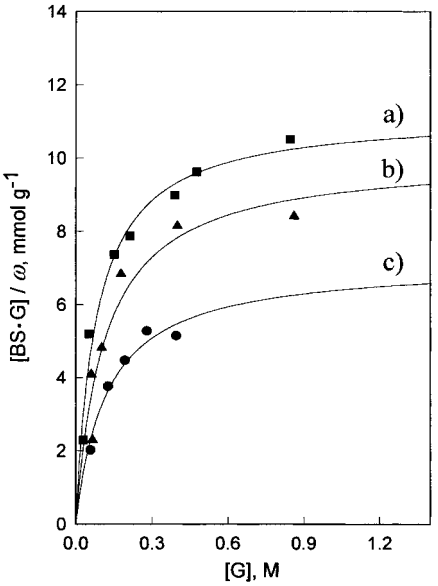

Figure 10. Binding of host solid **3** with organic guests: a) MeOH (■); b) PhOH (▲); c) EtOH (●).

respectively. The values of the binding constants K_f and the binding site ($[BS]_o/\omega$) are summarized in Table 4. The values of $[BS]_o/\omega$ indicate that the host solid **2** binds 1–6 guest organic molecules and that the host solid **3** binds 12–19 guest molecules per formula unit, depending on the guests. The total volumes of the bound guests per unit formula of **2** estimated from $[BS]_o/\omega$ values are 397 Å^3 for MeOH, 395 Å^3 for EtOH, and 161 Å^3 for PhOH. For the host solid **3**, they are 1280 Å^3 for MeOH, 1260 Å^3 for EtOH, and 2630 Å^3 for PhOH. This indicates that the total volumes of the maximum numbers of included guests are much greater (1.5–5.1 times) than the total cavity volume of the host solids (106 Å^3 for **2** and 514 Å^3 for **3**). As discussed later, the XRPD patterns indicate that the guests are included in the space between the layers (as evidenced by an increase in the cell dimensions) as well as inside the channels. The K_f values indicate that the host solid **2** binds guests in the order of MeOH > EtOH > PhOH and the host solid **3** binds guests in the order of MeOH > PhOH > EtOH. In terms of K_f values, the host solid **2** binds all three guests more strongly than the solid **3**. On the other hand, $[BS]_o/\omega$ values indicate that the solid **3** has greater capacity for binding the guest molecules.

The host–guest compounds were characterized by elemental analysis and IR spectra (Table S1 and Figures S5–S10 in the Supporting Information) as well as by XRPD patterns (Figure 11 and Figure 12). When the elemental analysis was carried out for the solid after immersing it in a solution of MeOH or EtOH in toluene, the data showed that far fewer MeOH and EtOH molecules than estimated from the $[BS]_o/\omega$ values were bound to the host solid (Table S1 in the Supporting Information). In the case of PhOH, however, the data indicated that the same numbers of PhOH molecules as estimated from $[BS]_o/\omega$ values were bound to the host (Table S1 in the Supporting Information). In particular, when the solid **3** was immersed in an aqueous solution of PhOH for 12 h instead of in toluene solution, the elemental analysis

0947-6539/01/0701-0310 $ 17.50+.50/0 *Chem. Eur. J.* **2001**, *7*, No. 1

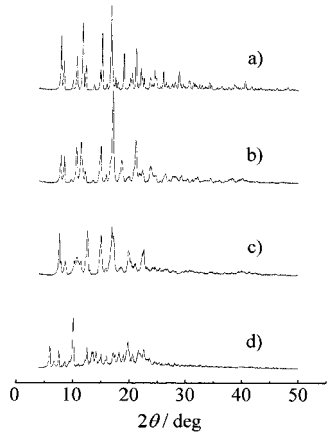

Figure 11. XRPD patterns of: a) original solid **2**; b) dried solid **2** binding MeOH; c) dried solid **2** binding EtOH; d) dried solid **2** binding PhOH.

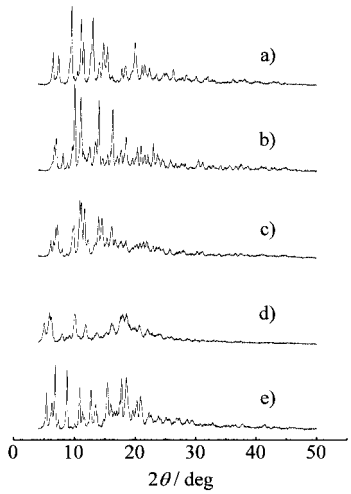

Figure 12. XRPD patterns of: a) original solid **3**; b) dried solid **3** binding MeOH; c) dried solid **3** binding EtOH; d) dried solid **3** binding PhOH; e) solid **3** binding PhOH in H_2O.

indicated that PhOH molecules were bound in addition to water molecules (Table S1 in the Supporting Information and Figure 12). The fact that the solid is able to bind PhOH even in water implies its potential application to remove PhOH from contaminated water.

The XRPD patterns for the guest-bound host solids **2** and **3** are presented in Figure 11 and Figure 12 and Tables S2–S3 in the Supporting Information, and the cell parameters estimated herefrom are summarized in Table 5. As seen in Table 5, all the guest-bound host solids show increased cell dimensions and volumes, contrary to the case of the copper(II) guest. This probably happens because the guest molecules are included between the layers as well as inside the channels. Interestingly, when the solids binding MeOH, EtOH, and PhOH were immersed in a MeCN/H_2O mixture for 30 min, exactly the same patterns as for the original host solid were regenerated (Figure S11 in the Supporting Information). This again implies that the host solids may be used as adsorbing materials for such organic molecules. Although we have tried to grow single crystals in which the guest molecules are included, we have not succeeded in obtaining single crystals suitable for X-ray diffraction studies.

In conclusion, we have assembled three-dimensional supramolecular networks by using a nickel(II) macrocyclic complex containing pendant pyridyl groups and *cis*,*cis*-1,3,5-cyclohexanetricarboxylic acid. The macrocyclic complex collectively induces metal–ligand coordination, hydrogen bonding, and $\pi-\pi$ stacking interactions to produce quite robust and insoluble solids. The solids selectively bind $[Cu(NH_3)_4](ClO_4)_2$ over $[Cu(en)_2](ClO_4)_2$ in MeCN solution and differentiate MeOH, EtOH, and PhOH in toluene.

Experimental Section

General methods: All chemicals and solvents used in the syntheses were of reagent grade and were used without further purification. For the inclusion studies, MeCN and toluene were dried with molecular sieves prior to use. Infrared spectra were recorded with a Perkin Elmer 2000 FTIR spectrophotometer. Elemental analyses were performed by the analytical laboratory of Seoul National University. UV/Vis diffuse reflectance spectra were recorded with a Cary 300 Bio UV/Vis spectrophotometer. Thermogravimetric analysis (TGA) and differential thermal analysis (DTA) were performed under N_2(g) at a scan rate of 5 °C min^{-1} using a Rigaku Tas-100 system. X-ray powder diffraction data were recorded on a Mac Science M18XHF-22 diffractometer at 50 kV and 100 mA for $Cu_{K\alpha}$ ($\lambda = 1.54050$ Å) with a scan speed of 5° min^{-1} and a step size of 0.02° in 2θ. Gas chromatographic (GC) experiments were conducted by using a HP 6890 Series GC system which was fitted with a 30 m × 0.25 mm × 0.25 μm cross-linked polydimethylsiloxane capillary column and interfaced with a GC ChemStation. The column temperature was programmed from 100 °C (5 min) to 300 °C (2 min) at the rate of 25 °C min^{-1}. A flame ionization detector was used.

Table 5. Cell constants for **2**, **3**, and their inclusion compounds.

Compound	a [Å]	b [Å]	c [Å]	α [°]	β [°]	γ [°]	V [Å^3]
2[a]	9.521	11.224	11.345	79.52	77.83	68.61	1096.1
2 · $[Cu(NH_3)_4](ClO_4)_2$[b]	9.611	11.296	11.444	79.25	77.07	68.32	1117.8
2 · MeOH[c]	10.194	12.244	13.037	64.61	94.51	66.92	1291.4
2 · EtOH[c]	11.051	12.382	13.394	113.17	89.08	53.36	1271.4
2 · PhOH[c]	9.921	14.053	18.434	55.56	109.80	101.44	1994.4
3[a]	12.570	14.714	15.015	108.33	108.42	91.66	2475.7
3 · $[Cu(NH_3)_4](ClO_4)_2$[b]	12.253	14.970	15.712	112.34	108.56	97.31	2423.7
3 · MeOH[c]	14.550	13.711	16.401	80.71	117.91	86.12	2814.6
3 · EtOH[c]	15.243	15.961	16.571	113.00	63.26	121.82	2996.2
3 · PhOH[c]	9.676	18.051	19.692	66.31	89.76	62.94	2736.5
3 · PhOH(H_2O)[d]	12.053	20.884	18.702	63.49	83.38	49.93	3120.4

[a] Original solid. [b] Inclusion of guest was made in MeCN. [c] Inclusion of guest was made in toluene. [d] Inclusion of guest was made in water. Cell parameters of inclusion compounds ([b], [c], and [d]) were determined by the TREOR computer program.

  0947-6539/01/0701-0311 $ 17.50+.50/0

Synthesis: **safety note**: Although we have experienced no problem with the compounds reported in this work, perchlorate salts of metal complexes with organic ligands are often explosive and should be handled with great caution.

$[Ni(L^1+2H)](ClO_4)_4\cdot 2H_2O$: Ethylenediamine (6.8 mL, 0.10 mol), paraformaldehyde (6.0 g, 0.20 mol), and 4-(aminomethyl)pyridine (10.8 g, 0.10 mol) were slowly added to a stirred solution of $Ni(OAc)_2\cdot 4H_2O$ (12.4 g, 0.05 mol) in methanol (75 mL). The mixture was heated under reflux for 24 h. The solution was filtered while hot and the filtrate was concentrated to about ⅕ of the original volume. $HClO_4$ (60%, 20 mL) was added to the yellow-brown solution and the solution was allowed to stand in a refrigerator until yellow crystals formed, which were filtered off, washed with methanol, and dried in air. Yield: 35%; FTIR (Nujol mull): $\tilde{\nu}=3543$(br s), 3212(s), 3175(s), 3100(s), 1640(s), 1600(s), 1505(s), 1100(s), 625(s) cm^{-1}; UV/Vis (H_2O): λ_{max} (ε) = 445 nm (54 $M^{-1}cm^{-1}$); elemental analysis calcd (%) for $NiC_{20}H_{38}N_8Cl_4O_{18}$ (879.07): C 27.33, H 4.36, N 12.75; found: C 26.90, H 3.92, N 12.52.

$[Ni(L^1)](ClO_4)_2\cdot 2H_2O$ (1): An excess amount of triethylamine (2 mL) was added to a suspension of $[Ni(\mathbf{L^1}+2H)](ClO_4)_4\cdot 2H_2O$ (2.5 g) in MeCN (40 mL). The complex dissolved in the solution and yellow crystals of $[Ni(L^1)](ClO_4)_2\cdot 2H_2O$ formed in a few minutes. The crystals were filtered off, washed with water, and dried in air. Crystals suitable for the X-ray diffraction study were obtained by recrystallization of the compound in hot water. Yield: 90%; FTIR (Nujol mull): $\tilde{\nu}=3590$(br s), 3195(s), 1650(m), 1605(s), 1565(m), 1100(s), 625(s) cm^{-1}; UV/Vis ($MeNO_2$): λ_{max} (ε) = 450 nm (68 $M^{-1}cm^{-1}$); elemental analysis calcd (%) for $NiC_{20}H_{36}N_8Cl_2O_{10}$ (678.15): C 35.42, H 5.35, N 16.52; found: C 35.24, H 4.93, N 16.59.

$[Ni(C_{20}H_{32}N_8)][C_6H_9(COOH)_2(COO)]_2\cdot 4H_2O$ (2): The nickel(II) complex **1** (0.17 g, 0.245 mmol) was dissolved in a mixture of MeCN and H_2O (1:1 v/v, 12 mL), and a solution containing *cis*,*cis*-1,3,5-cyclohexanetricarboxylic acid (H_3CTC) (0.11 g, 0.49 mmol) and pyridine (0.8 mL) in MeCN (6 mL) was added dropwise. The pink solution was allowed to stand at room temperature until pale pink crystals formed, which were filtered off, washed with MeCN/H_2O, and dried in air. Yield: 78%; FTIR (Nujol mull): $\tilde{\nu}=3479$ (br s), 3284 (s), 3175 (s), 2539 (br m), 1958 (br m), 1713 (s), 1692 (s), 1611 (s), 1567 (s), 1243 (s), 1180 (s), 980 (s), 851 (s), 793 (s), 654 (s) cm^{-1}; UV/Vis (diffuse reflectance spectrum): $\lambda_{max}=267$, 335, 507, 640 nm; elemental analysis calcd (%) for $NiC_{38}H_{62}N_8O_{16}$ (945.66): C 48.27, H 6.61, N 11.85; found: C 48.33, H 6.65, N 12.17.

$[Ni(C_{20}H_{32}N_8)]_3[C_6H_9(COO)_3]_2\cdot 16H_2O$ (3): A solution containing *cis*,*cis*-1,3,5-cyclohexanetricarboxylic acid (H_3CTC) (0.022 g, 0.098 mmol) and an excess amount of triethylamine (0.3 mL) in MeCN (5 mL) was added dropwise to a solution of **1** (0.10 g, 0.15 mmol) in MeCN/H_2O (1:1 v/v, 10 mL). The resulting pink solution was allowed to stand at room temperature until pale pink crystals formed, which were filtered off, washed with MeCN/H_2O, and dried in air. Yield: 70%; FTIR (Nujol mull): $\tilde{\nu}=3364$ (br s), 3229 (s), 3147 (s), 1651 (m), 1605 (s), 1556 (s), 1385 (s), 1344 (s), 1276 (s), 1219 (m), 1182 (m), 1150 (m), 1030 (s), 998 (s), 914 (m), 859 (m), 802 (s), 770 (m), 739 (m) 643 (m) cm^{-1}; UV/Vis (diffuse reflectance spectrum): $\lambda_{max}=260$, 332, 509, 655 nm; elemental analysis calcd (%) for $Ni_3C_{78}H_{146}N_{24}O_{28}$ (2044.23): C 45.83, H 7.20, N 16.44; found: C 45.71, H 6.89, N 16.42.

X-ray diffraction measurements: Single crystals were mounted on an Enraf–Nonius CAD4 diffractometer. The unit cell parameters were determined from 25-machine-centered reflections with $20<2\theta<27^\circ$ for **1**, $22<2\theta<26^\circ$ for **2**, and $22<2\theta<25^\circ$ for **3**. Intensities were collected with graphite-monochromated $Mo_{K\alpha}$ radiation, using the $\omega-2\theta$ scan. Three standard reflections were measured every 2 h as orientation and intensity control and no significant intensity decay was observed. Data were corrected for Lorentz and polarization effects. Absorption correction was not made. For **1**, among 2523 reflections measured in the range $4.36<2\theta<49.94^\circ$, 1897 were assumed to be observed ($F>4\sigma(F)$). For **2**, among 3756 reflections measured in the range $3.70<2\theta<49.92^\circ$, 3432 were assumed to be observed ($F>4\sigma(F)$). For **3**, among 7471 reflections measured in the range $3.46<2\theta<50.44^\circ$, 4300 were assumed to be observed ($F>4\sigma(F)$). The crystal structures were solved by direct methods[31] for **1** and **3** and by Patterson methods[31] for **2**, and refined by full-matrix least-squares refinement using the SHELXL-97 computer program.[32] All non-hydrogen atoms in **1**, **2**, and **3** were refined anisotropically, except N4B, C6B, C7B, C8B, C9B, and C10B in **3** which have large thermal disorder. For **1** and **3**, the positions of all hydrogen atoms were allowed to ride on their bonded atoms with the isotropic displacement factors fixed with values 1.2 times those of the bonded atoms. The aqua hydrogen atoms in **1** were located from the difference Fourier maps and refined with isotropic displacement factors. For **2**, acid protons were located from the difference Fourier maps and refined isotropically and the remaining hydrogen atoms were positioned geometrically and refined by using a riding model. The crystallographic data of **1**–**3** are summarized in Table 6. Crystallographic data (excluding structure factors) for the structures reported in this paper have been deposited with the Cambridge Crystallographic Data Centre as supplementary publication nos. CCDC-141617 (**1**), CCDC-141618 (**2**), and CCDC-141619 (**3**). Copies of the data can be obtained free of charge on application to CCDC, 12 Union Road, Cambridge CB2 1EZ, UK (fax: (+44) 1223 336–033; e-mail: deposit@ccdc.cam.ac.uk).

Binding of 2 and 3 with copper(II) complexes: The formation constant K_f for the complexes formed between a binding site (BS) of the insoluble hosts and a guest molecule (G) can be defined as k_{ad}/k_{de} [Eq. (1)] by analogy with the Langmuir isotherm for adsorption of gas molecules on solid surfaces.[21, 30] Plots of the concentration of G bound to BS ([BS·G]) against [G] were made and the K_f value and $[BS]_o$ values were estimated by the analysis of the data according to Equation (2). In the experiment, total concen-

Table 6. Crystallographic data for the compounds **1**–**3**.

Compound	**1**	**2**	**3**
chemical formula	$NiC_{20}H_{36}N_8Cl_2O_{10}$	$NiC_{38}H_{62}N_8O_{16}$	$Ni_3C_{78}H_{146}N_{24}O_{28}$
formula weight	678.15	945.66	2044.23
crystal system	monoclinic	triclinic	triclinic
space group	$P2_1/c$	$P\bar{1}$	$P\bar{1}$
a [Å]	9.489(1)	9.521(1)	12.570(2)
b [Å]	8.757(1)	11.224(2)	14.714(3)
c [Å]	17.527(2)	11.345(2)	15.015(3)
α [°]		79.52(1)	108.33(2)
β [°]	99.96(1)	77.83(1)	108.42(2)
γ [°]		68.61(1)	91.66(1)
V [Å^3]	1434.4(2)	1096.1(3)	2475.7(8)
Z	2	1	1
ρ_{calcd} [g cm^{-3}]	1.570	1.433	1.371
λ [Å]	0.71069	0.71069	0.71069
μ [mm^{-1}]	0.929	0.522	0.649
temperature [K]	293	293	293
GOF	1.028	1.077	0.896
F(000)	708	502	1090
no. of data collected	2750	4051	7877
no. of unique data	2523	3756	7471
no. of obsd data [$F>4\sigma(F)$]	1897	3432	4300
no. of variables	195	294	574
R_1[a] (4σ data)	0.0523	0.0556	0.0774
wR_2[b] (4σ data)	0.1503	0.1453	0.1823

[a] $R_1=\Sigma||F_o|-|F_c||/\Sigma|F_o|$. [b] $wR_2(F^2)=[\Sigma w(F_o^2-F_c^2)^2/\Sigma w(F_o^2)^2]^{1/2}$. $w=1/[\sigma^2(F_o^2)+(0.1156P)^2]$, where $P=(F_o^2+2F_c^2)/3$ for **1**. $w=1/[\sigma^2(F_o^2)+(0.1216P)^2+0.1073P]$, where $P=(F_o^2+2F_c^2)/3$ for **2**. $w=1/[\sigma^2(F_o^2)+(0.1463P)^2]$, where $P=(F_o^2+2F_c^2)/3$ for **3**.

0947-6539/01/0701-0312 $ 17.50+.50/0 *Chem. Eur. J.* **2001**, *7*, No. 1

tration of guest ($[G]_o$) was varied to keep the θ values ranging between 20 and 80%.

$$BS + G \underset{k_{de}}{\overset{k_{ad}}{\rightleftharpoons}} BS \cdot G$$

$$K_f = \frac{k_{ad}}{k_{de}} = \frac{[BS \cdot G]}{[BS][G]} \quad (1)$$

If θ is defined as fractional coverage,

$$\theta = \frac{[BS \cdot G]}{[BS]_o} = \frac{[G]}{([G] + 1/K_f)}$$

$$\text{then } \frac{[BS \cdot G]}{\omega} = \frac{([BS]_o/\omega)[G]}{([G] + 1/K_f)} \quad (2)$$

where ω is amount of host solid per unit volume of the solution ($mg\,mL^{-1}$). Freshly prepared pink crystals of **2** and **3** were ground in a mortar until they became microcrystalline powder. The solid sample (50–100 mg) whose weight was accurately measured was immersed in the MeCN solutions (5 mL) of $[Cu(en)_2](ClO_4)_2$ and $[Cu(NH_3)_4](ClO_4)_2$, respectively, for 24 h at 25 °C. The initial concentrations of the copper(II) complexes were varied as 5.61×10^{-3}–2.82×10^{-2} M for **2** and 6.48×10^{-4}–3.46×10^{-2} M for **3** to keep the θ value 0.2–0.8. The absorption changes of the complexes were measured spectrophotometrically, and the data were fitted to Equation (2). The time attaining the equilibrium for the host–guest complex formation was estimated by monitoring the change of the guest concentration spectrophotometrically. A typical time dependency of a guest binding is shown in Figure S12 in the Supporting Information. According to this, we assumed that the equilibrium could be reached in 24 h.

Binding of 2 and 3 with organic guests: Pale pink crystals of **2** and **3** were ground in a mortar until they became a microcrystalline powder and then they were dried at 80 °C under vacuum for 6 h. The solid (20–50 mg) whose weight was measured exactly was immersed in the toluene solutions (1.0–2.5 mL) containing benzene, methanol, ethanol, and phenol, respectively, for 7 h at 30 °C. The initial concentrations of methanol, ethanol, and phenol were varied as 1.44×10^{-1}–2.09 M, $(0.98$–$5.0) \times 10^{-1}$ M, and 3.00×10^{-2}–1.23 M, respectively, to keep the θ values ranging 20–80%. The concentration changes of the organic guests were measured by GC using dodecane as the internal standard. The data were fitted to Equation (2). A typical time dependency of a guest binding is represented in Figure S13 in the Supporting Information. According to the data, we assumed that the equilibrium could be attained within 7 h.

Acknowledgements

This work was supported by the Korea Science and Engineering Foundation (1999-1-122-001-5) and the Center for Molecular Catalysis.

[1] a) D. B. Amabilino, J. F. Stoddart, *Chem. Rev.* **1995**, *95*, 2725; b) J.-M. Lehn, *Supramolecular Chemistry*: *Concepts and Perspectives*, VCH, Weinheim, **1995**; c) D. S. Lawrence, T. Jiang, M. Levett, *Chem. Rev.* **1995**, *95*, 2229; d) T. Iwamoto in *Inclusion Compounds*, *Vol. 5* (Eds.: J. L. Atwood, J. E. D. Davies, D. D. MacNicol), Academic Press, London, **1991**, pp. 177–212.

[2] P. Bhyrappa, S. R. Wilson, K. S. Suslick, *J. Am. Chem. Soc.* **1997**, *119*, 8492.

[3] a) J. Ranford, J. J. Vittal, D. Wu, *Angew. Chem.* **1998**, *110*, 1159; *Angew. Chem. Int. Ed.* **1998**, *37*, 1114; b) K. Kobayashi, M. Koyanagi, K. Endo, H. Masuda, Y. Aoyama, *Chem. Eur. J.* **1998**, *4*, 417; c) T. Dewa, K. Endo, Y. Aoyama, *J. Am. Chem. Soc.* **1998**, *120*, 8933.

[4] W. T. S. Huck, R. Hulst, P. Timmerman, F. C. Veggel, D. N. Reinhoudt, *Angew. Chem.* **1997**, *109*, 1046; *Angew. Chem. Int. Ed. Engl.* **1997**, *36*, 1006.

[5] a) M. Fujita, Y. J. Kwon, O. Sasaki, K. Yamaguchi, K. Ogura, *J. Am. Chem. Soc.* **1995**, *117*, 7287; b) M. Fujita, M. Aoyagi, F. Ibukuro, K. Ogura, K. Yamaguchi, *J. Am. Chem. Soc.* **1998**, *120*, 611.

[6] G. B. Gardner, D. Venkataraman, J. S. Moore, S. Lee, *Nature*, **1995**, *374*, 792.

[7] P. R. Ashton, A. N. Collins, M. C. T. Fyfe, S. Menzer, J. F. Stoddart, D. J. Williams, *Angew. Chem.* **1997**, *109*, 760; *Angew. Chem. Int. Ed. Engl.* **1997**, *36,* 735.

[8] C. Janiak, *Angew. Chem.* **1997**, *109*, 1499; *Angew. Chem. Int. Ed. Engl.* **1997**, *36*, 1431.

[9] J. A. Real, E. Andrés, M. C. Muñoz, M. Julve, T. Granier, A. Bousseksou, F. Varret, *Science*, **1995**, *268*, 265.

[10] O. R. Evans, R.-G. Xiong, Z. Wang, G. K. Wong, W. Lin, *Angew. Chem.* **1999**, *111*, 557; *Angew. Chem. Int. Ed.* **1999**, *38*, 536.

[11] O. M. Yaghi, H. Li, T. L. Groy, *J. Am. Chem. Soc.* **1996**, *118*, 9096.

[12] a) S. Subramanian, M. J. Zaworotko, *Angew. Chem.* **1995**, *107*, 2295; *Angew. Chem. Int. Ed. Engl.* **1995**, *34,* 2127; b) T. L. Hennigart, D. C. Macquarrie, P. Losier, R. D. Rogers, M. J. Zaworotko, *Angew. Chem.* **1997**, *109*, 1044; *Angew. Chem. Int. Ed. Engl.* **1997**, *36*, 972.

[13] M. Fujita, Y. J. Kwon, S. Washizu, K. Ogura, *J. Am. Chem. Soc.* **1994**, *116*, 1151.

[14] a) O. M. Yaghi, C. E. Davis, G. Li, H. Li, *J. Am. Chem. Soc.* **1997**, *119*, 2861; b) O. M. Yaghi, H. Li, *J. Am. Chem. Soc.* **1995**, *117*, 10401; c) O. M. Yaghi, G. Li, H. Li, *Nature,* **1995**, *378*, 703; d) O. M. Yaghi, Z. Sun, D. A. Richardson, T. L. Groy, *J. Am. Chem. Soc.* **1994**, *116,* 807.

[15] D. Venkataraman, G. B. Gardner, S. Lee, J. S. Moore, *J. Am. Chem. Soc.* **1995**, *117*, 11600.

[16] M. Kondo, T. Yoshitomi, K. Seki, H. Matsuzaka, S. Kitagawa, *Angew. Chem.* **1997**, *109*, 1844; *Angew. Chem. Int. Ed. Engl.* **1997**, *36*, 1725.

[17] T. Sawaki, T. Dewa, Y. Aoyama, *J. Am. Chem. Soc.* **1998**, *120*, 8539.

[18] a) H. Li, C. E. Davis, T. L. Groy, D. G. Kelley, O. M. Yaghi, *J. Am. Chem. Soc.* **1998**, *120*, 2186; b) H. Li, M. Eddaoudi, D. A. Richardson, O. M. Yaghi, *J. Am. Chem. Soc.* **1998**, *120*, 8567; c) H. Li, M. Eddaoudi, T. L. Groy, O. M. Yaghi, *J. Am. Chem. Soc.* **1998**, *120*, 8571.

[19] a) B. F. Hoskins, R. Robson, D. A. Slizys, *J. Am. Chem. Soc.* **1997**, *119*, 2952; b) C. J. Kepert, M. J. Rosseinsky, *Chem. Commun.* **1998**, 31; c) S. R. Batten, R. Robson, *Angew. Chem.* **1998**, *110*, 1558; *Angew. Chem. Int. Ed.* **1998**, *37*, 1461; d) W. Lin, O. R. Evans, R.-G. Xiong, Z. Wang, *J. Am. Chem. Soc.* **1998**, *120*, 13272; e) B. F. Abrahams, S. R. Batten, M. J. Grannas, H. Hamit, B. F. Hoskins, R. Robson, *Angew. Chem.* **1999**, *111*, 1538; *Angew. Chem. Int. Ed.* **1999**, *38*, 1475.

[20] H. J. Choi, M. P. Suh, *J. Am. Chem. Soc.* **1998**, *120*, 10622.

[21] H. J. Choi, T. S. Lee, M. P. Suh, *Angew. Chem.* **1999**, *111*, 1490; *Angew. Chem. Int. Ed.* **1999**, *38*, 1405.

[22] M. P. Suh, B. Y. Shim, T. S. Yoon, *Inorg. Chem.* **1994**, *33*, 5509.

[23] M. P. Suh, I. S. Kim, B. Y. Shim, D. Hong, T.-S. Yoon, *Inorg. Chem.* **1996**, *35*, 3595.

[24] M. P. Suh, *Adv. Inorg. Chem.* **1996**, *44*, 93.

[25] M. P. Suh, M. Y. Han, J. H. Lee, K. S. Min, C. Hyeon, *J. Am. Chem. Soc.* **1998**, *120*, 3819.

[26] R. D. Hancock, *Acc. Chem. Res.* **1990**, *23*, 253.

[27] a) G. R. Desiraju, *Crystal Engineering: The Design of Organic Solids*, Elsevier, New York, **1989**, Chapter 4; b) C. A. Hunter, J. Singh, J. M. Thornton, *J. Mol. Biol.* **1991**, *218*, 837; c) A. S. Shetty, J. Zhang, J. S. Moore, *J. Am. Chem. Soc.* **1996**, *118*, 1019.

[28] F. L. Urbach in *Coordination Chemistry of Macrocyclic Compounds* (Eds.: G. A. Melson), Plenum, New York, **1979**, pp. 350–355.

[29] A. L. Spek, PLATON99, A Multipurpose Crystallographic Tool, Utrecht University, Utrecht, The Netherlands, **1999**.

[30] a) P. W. Atkins, *Physical Chemistry*, 4th ed., Oxford University Press, Oxford, **1990**, pp. 885–888; b) B.-B. Jang, K.-P. Lee, D.-H. Min, J. Suh, *J. Am. Chem. Soc.* **1998**, *120*, 12008; c) J. Suh, H. S. Park, *J. Polym. Sci. A*: *Polym. Chem.* **1997**, *35*, 1197.

[31] G. M. Sheldrick, *Acta Crystallogr. Sect. A* **1990**, *46*, 467.

[32] G. M. Sheldrick, SHELXL97, program for the crystal structure refinement, University of Göttingen, Germany, **1997**.

Received: March 23, 2000
Revised: July 31, 2000 [F2381]